High-Sensitive Numerical Gas Detection Using LSPR Effect and Fano Resonance in a Slotted MDM Structure

Hai LIU, Benlei ZHAO, Xu ZHANG, Hancheng ZHANG, Bo WU, and Shoufeng TANG*

School of Information and Control Engineering, China University of Mining and Technology, Xuzhou 221116, China

*Corresponding author: Shoufeng TANG   E-mail: sieedksft@cumt.edu.cn

Abstract: A high-sensitive numerical measurement of methane based on the combined use of the localized surface plasmon resonance (LSPR) and Fano resonance in a slotted metal-dielectric-metal (MDM) periodic structure is numerically investigated. A groove is etched in an original MDM structure to excite the diploe mode at both sides of the groove, and the coherent coupling of two dipole modes is enhanced to realize a fast response, which is beneficial to gas-sensing. The influence of geometric parameters on the reflection spectra and methane sensitivity are analyzed to obtain optimal geometry. Moreover, an etching ring is introduced on the top metal to further raise the coupling area and coupling strength. The Fano resonance is subtly integrated into the optimized structure with asymmetry to achieve greater gas sensitivity. After the introduction of the Fano resonance, the field enhancement caused by the LSPR effect becomes greater and the methane sensitivity can reach up to 8.421 nm/% in numerical calculations, which increases 56.8% more than that of the original one. The combined use of the LSPR and Fano resonance in an optimized MDM structure provides an effective method for high-sensitive gas detection.

Keywords: Localized surface plasmon resonance; Fano resonance; gas sensors; MDM structure

1. Introduction

Surface plasmon polariton (SPP) [1, 2] is a type of light wave which propagates along with the separation between a dielectric and a metal. Its unique optical characteristics make it overcome the diffraction limit of conventional optical devices. In particular, local surface plasmon resonance (LSPR) [3–5] generally occurs within metallic nanostructures, and the LSPR can effectively control the propagation of free waves and realize the local field electromagnetic enhancement [6, 7]. Since the LSPR is highly sensitive to the dielectric environment's variation, a growing number of LSPR-based devices have been investigated for various gas-sensing applications. Yang *et al.* [8, 9] reported a methane sensor based on the surface plasmon resonance (SPR) theory, with a sensitivity of 1.078 nm/%. In 2018, Liu *et al.* [10] proposed a PCF (photonic crystal fiber)-SPR structure for methane and hydrogen detection, and gas sensitivities were 1.99 nm/% and 0.19 nm/%, respectively. However, the gas-sensitive film is hardly coated onto the inner surface of the PCF-SPR structure, and the diffusion of gas in cladding air holes is relatively slow. Therefore, it is essential to explore an effective sensing method for gas detection to enhance the sensitivity while the coating

fabrication can be simplified. The present sensing principle is mostly based on detecting the resonant peak of spectra. The gas concentration can be calculated through quantifying the shift of the resonant wavelength. Compared with the SPR sensors, the LSPR sensors have outstanding local field enhancement and higher sensitivity to the dielectric environment, which is beneficial for gas detections. The dependence opens up a gas detection approach based on the relationship between the refractive index of gas-sensitive materials and the resonance peak-shifts [11].

Recently, the nanostructures play an important role in designing sensors and absorbers [12–16], especially for the metal-dielectric-metal (MDM) structure. Since the antiparallel surface currents exist on the top and bottom metals, a strong electromagnetic coupling is appropriate for the absorber or sensing systems. In 2017, Liu *et al.* [17] designed an ultra-wideband absorber based on MDM nanostructure. In the following year, Lei *et al.* [18] proposed a near-infrared MDM absorber, and the average absorption could reach 97%. In 2020, Bazgir *et al.* [19] designed a refractive index sensor based on a metal-insulator-metal (MIM) coupled waveguide with a sensitivity of about 1260 nm/RIU and figure of merit (FOM) of 120 RIU^{-1}. Chao *et al.* [20] proposed a high-sensitive refractive-index sensor based on the MIM structure with a sensitivity of 3 500 nm/RIU. In 2021, Mahmud *et al.* [21] designed a plasmonic sensor based on the metal-insulator-metal structure, which was composed of a straight waveguide and a resonator, with a sensitivity of 2713 nm/RIU and FOM of 35.1 [21]. Inspired by the reported methods, we use the gas-sensitive film as the dielectric of the MDM structure. The high concentration of the electric field enables the resonant wavelength to have a large shift even though the refractive-index of the gas-sensitive film changes very little. The fabrication technique is much simpler than those of traditional fiber gas-sensors, whose gas-sensitive film is coated on the cladding air-hole.

Because of the high sensitivity of the Fano resonance to a tiny change of surrounding material, the introduction of the Fano resonance provides a new way to enhance the sensitivity [22, 23]. As is known, the asymmetry can hybridize different plasmon resonances, which promotes the coupling between the wider and narrower plasmon resonances to produce the Fano resonance. The plasmonic modes with net dipole moment can interact with the external electromagnetic field, which is also known as bright modes. However, dark modes with zero net dipole moment radiate extremely weakly, making them hardly interact with the external electromagnetic filed. Notably, the dark modes cannot be excited by light, but they can be excited by the near-filed coupling with bright modes. The dark modes interact with bright modes through the near-field coupling which produces the Fano resonance. Here, the excitement of dark modes and interaction between bright and dark modes can be realized due to the asymmetry of the nanostructure. Compared with local plasmon resonance, the Fano resonance has a reinforcing effect on electromagnetic field enhancement.

In 2019, we [24] proposed an LSPR methane sensor based on a hexagonal gold nanoring array with a sensitivity of –1.04 nm/%. However, the sensitivity may not meet the demand for the detections in some harsh circumstances. High-sensitive methane sensors are still needed. Here, an effective method is proposed to enhance the gas sensitivity through the combined use of the MDM structure and Fano resonance. Firstly, we design a simple MDM structure with a slit in the middle dielectric layer and the top metal layer to excite the dipole mode and generate coherent coupling in the grove, which produces a strong electric field. After introducing an etching ring, the proposed sensor achieves a fast response by expanding the reaction area. An increase in the coupling area and intensity is very beneficial to enhance the sensitivity. The

reason is that the Fano resonance superimposed original plasmon resonance and the electrical field enhancement is also stronger than the previous one. The gas sensitivity under the combined effect of the LSPR and Fano resonance is higher than that under the LSPR effect only. Numerical simulation results show that the maximum methane sensitivity of improved structure can reach up to 8.4214 nm/%, which further increases 56.8% than the original value.

2. Sensing principle and model optimization

The electron in the noble metal will collectively oscillate locally when the incident light interacts with the nanoparticle. The plasmon resonance peak is dependent on the geometric morphology, size, metal type, and surrounding medium. The dispersion relationship of the LSPR is demonstrated in (1), where l is the depth of penetration, and ε_1 and ε_2 are the permittivities of Au and the surrounding medium, respectively. The resonance frequency w_s is derived from (2), in which ω_p represents the angular frequency of surface plasmons. Equation (3) implies that the frequency is greatly dependent on the permittivity of the medium illustrated by the Drude-model, in which γ corresponds to the damping coefficient of the material. Equation (4) is a result of $\gamma \ll \omega_p$ in the region of low frequency. At $\varepsilon_1 = 2\varepsilon_m$, the LSPR frequency ω_{max} and LSPR wavelength λ_{max} can be described in (5). Based on the formula $\varepsilon_m = n_m^2$, (6) indicates an equivalent relationship when the frequency is converted to the wavelength. Above all, ε_m and n_m represent the dielectric constant and refractive index of the surrounding medium, respectively. λ_p can be seen as the isochronous elementary frequency of the corresponding bulk metal. As a result, there exists a linear relationship between the plasmon resonance wavelength and the refractive index.

$$\frac{\varepsilon_1}{\varepsilon_2} + \frac{l+1}{l} = 0 \qquad (1)$$

$$\omega_s = \omega_p \sqrt{\frac{1}{\varepsilon_s(l+1)+1}} \qquad (2)$$

$$\varepsilon_1 = 1 - \frac{\omega_p^2}{\omega^2 + \gamma^2} \qquad (3)$$

$$\varepsilon_1 = 1 - \frac{\omega_p^2}{\omega} \qquad (4)$$

$$\omega_{max} = \frac{\omega_p}{\sqrt{2\varepsilon_m + 1}} \qquad (5)$$

$$\lambda_{max} = \lambda_p \sqrt{2n_m^2 + 1}. \qquad (6)$$

Figure 1 demonstrates the proposed LSPR sensor structure (Structure A) which is composed of a periodic triple-layer array. Such an MDM array can be fabricated on a clean quartz substrate by the laser holographic lithography technology [25]. Especially, we make the upper metal layer smaller than the middle gas-sensitive layer to increase the reaction area and achieve a faster response. The groove is etched in the top and middle layers to enhance the response efficiency and electric field. Since the two dipole modes on both sides of the groove are coherent, a strong electrical field enhancement occurs in the groove and the middle gas-sensitive film, which provides a potential application in gas sensing. The geometry parameters are defined in Figs. 1(b) and 1(c), where P is the period of the array, h_1 is the thickness of the top gold film, h_2 is the thickness of the dielectric spacer, h_3 is the thickness of the bottom fold film, d is the length of the top square gold, and w is the width of the grove. The dielectric constant of Au is obtained by the Drude model $\varepsilon = 1 - \omega_p^2 / \omega(\omega + i\gamma_0)$, in which the plasmon frequency is $\omega_p = 1.37 \times 10^{16}$ s^{-1} and the collision frequency is $\gamma_0 = 4.08 \times 10^{13}$ s^{-1} [26]. The source shape is selected as a periodic plane wave with a polarization vector parallel to the x-direction. A series of simulations for the proposed nanostructure is carried out through the finite-difference time domain (FDTD) solution packages. As the proposed nanostructure is periodic, the periodic boundary condition is used in the x-direction and y-direction while the boundary

condition in the *z*-direction is the perfect match layer (PML). The sensing characteristics will be acquired by analyzing the plasmon resonance peak-shifts under various geometric parameters.
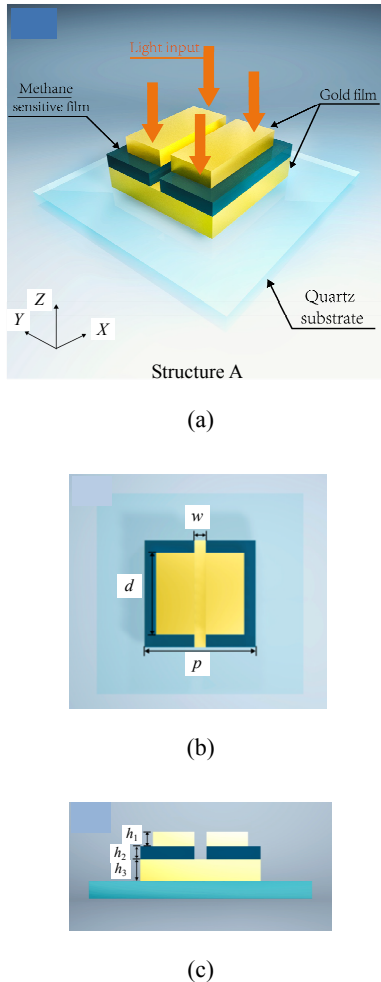

Structure A

(a)

(b)

(c)

Fig. 1 Schematic structure of the MDM unit cell: (a) 3-dimemsional (3D) view, (b) top view, and (c) side view of the structure.

The influence of the proposed nanostructure's geometric parameters on sensitivity is analyzed by calculating the reflection peak shifts. In analogous calculations, the thickness of the sensitive film (h_2) always keeps at 10 nm. We change the top metal length (d) from 700 nm to 780 nm and vary the thickness of the top metal (h_1) from 10 nm to 40 nm with an increment of 10 nm, and an increase in the width of the grove (w) from 10 nm to 40 nm to

optimize the structure. As the bottom metal can be seen as a mirror, it prohibits the transmission of the electromagnetic, so it is unnecessary to take the thickness of the bottom metal layer into account. The methane-sensitive material can be prepared by using cryptophane A with ultraviolet curable fluoro-siloxane (UVCFS). A dilute solution is applied to the surface of the metal layer, and then the surface of the film is polished with a nitrogen stream of 0.4 MPa. It is relatively feasible to coat the gas-sensitive composite film on the underlying metal by the capillary dip layer technique. Different from conventional gas sensors, the proposed sensor structure has higher sensitivity without interference of other gases. The spectral response to the target gas can be enhanced by optimizing the structural parameters. Such gas-sensitive film has a good repeatability and linear relationship between the refractive index n_{eff} and methane concentration C_{CH_4} within a range from 0% to 3.5% [9], as is expressed in (7):

$$n_{\text{eff}} = 1.447\,8 - 0.003\,8 C_{\text{CH}_4}. \tag{7}$$

Figure 2(a) demonstrates the sensitivity of the individual nanostructure with various values of groove width (w). The influence of the groove width is very little and the sensitivity can reach the maximum when $w = 20$ nm. Therefore, we single out the groove with a width of 20 nm for further research at first. Figures 2(b) and 2(c) demonstrate the sensitivity under different values of d and h_1. Obviously, the gas sensitivity is greatly affected by the metallic square's thickness rather than the length. With an increase in d, the local electric field gets enhanced, and the methane sensitivity increases. However, the sensitivity decreases as h_1 increases. The methane sensitivities under different values d and h_1 when $w = 20$ nm, $h_2 = 10$ nm, and $h_3 = 25$ nm are obtained in Table 1. The methane sensitivity can reach up to 7.30 nm/% when we select $d = 780$ nm and $h_1 = 30$ nm.
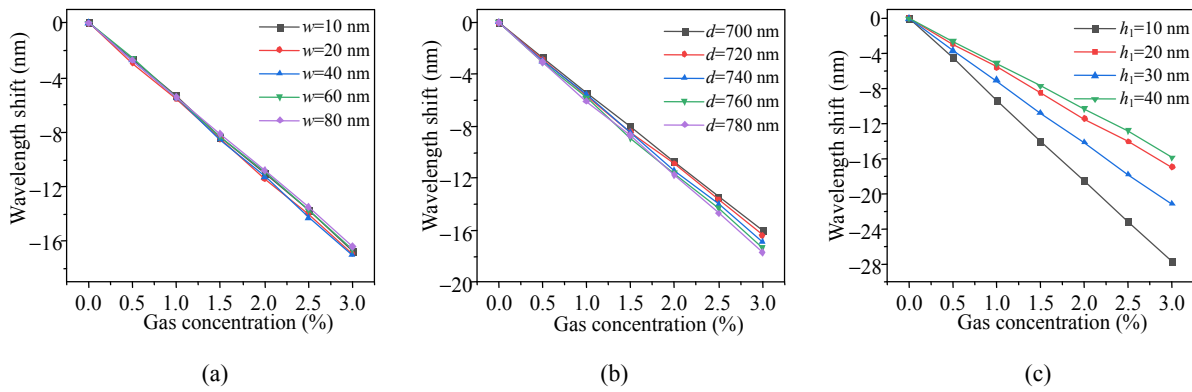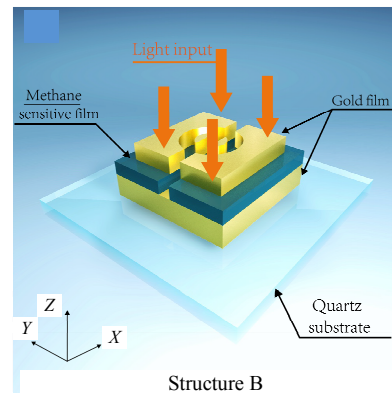
Fig. 2 Methane sensitivities under different values of (a) slit width, (b) length of top metal, and (c) thickness of top metal.

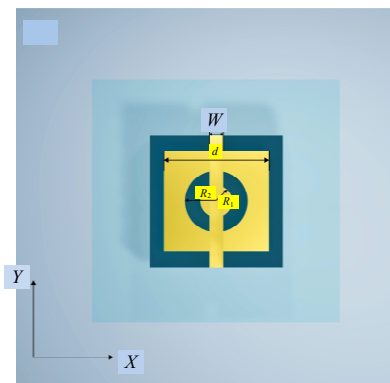Table 1 Methane sensitivities under different values of d and h_1 at $w = 20$ nm.

Group number	Top length d (nm)	Top thickness h_1 (nm)	Sensitivity (nm/%)
A_1	700	20	5.35
A_2	740	20	5.62
A_3	780	20	5.87
A_4	700	30	6.64
A_5	740	30	7.03
A_6	**780**	**30**	**7.30**
A_7	700	40	4.87
A_8	740	40	5.21
A_9	780	40	5.24

However, we still need a further optimization for the investigation. We introduce an etching ring with an outer radius $R_2 = 240$ nm and an inner radius $R_1 = 100$ nm into the top metal layer. After introducing an etching ring, the proposed structure achieves a fast response through increasing the reaction area. Since the LSPR generated by the ring resonance cavity enhances the coupling area and intensity, it is very beneficial to improve the sensitivity. The improved structure, schematically demonstrated in Fig. 3, can be formed through nanoring template lithography. Table 2 records the whole calculated results. The results show there is a significant increase in sensitivity compared with the

last groups. Accordingly, the improved nanostructure under $d = 780$ nm and $h_1 = 30$ nm can achieve the maximum sensitivity of 7.81 nm/%.
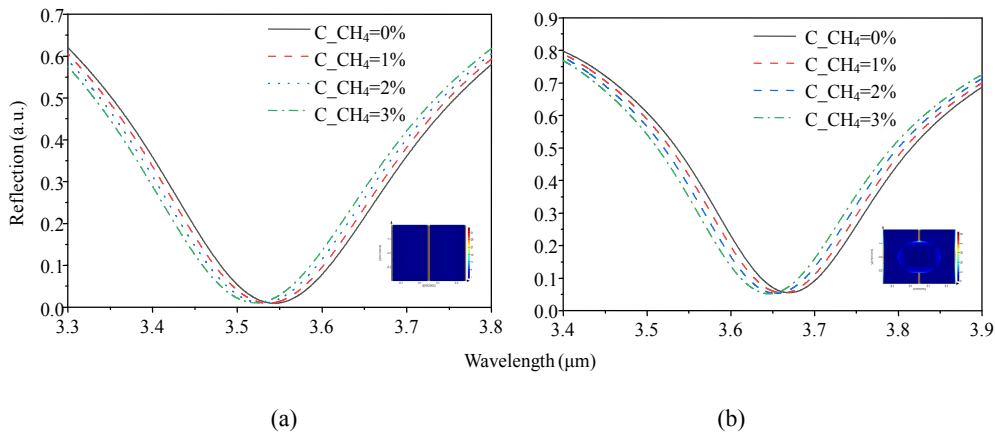

Structure B

(a)

(b)

Fig. 3 Schematic structure of improved structure (Structure B): (a) 3D view and (b) top view.

Table 2 Methane sensitivities for Structure B and the comparison with Structure A.

Group number	Top length d (nm)	Top thickness h_1 (nm)	Sensitivity (nm/%)	Increased rate (%)
B_1	700	20	5.99	12.0
B_2	740	20	6.30	11.9
B_3	780	20	6.43	9.5
B_4	700	30	7.25	9.2
B_5	740	30	7.59	7.97
B_6	**780**	**30**	**7.81**	**7.0**
B_7	700	40	5.23	7.4
B_8	740	40	5.37	3.1
B_9	780	40	5.62	7.9

For example, Fig. 4 presents the improved structure's reflection spectra at $d = 780$ nm , $h_1 = 30$ nm , and $w = 20$ nm , which are corresponding to the mentioned groups A_6 and

B_6 . It is clear that the refection intensity of the improved structure is greater than those of Structure A for the majority of plasmon excitation wavelengths, particularly at the plasmon resonance wavelength in Fig. 4. It can be explained that the etching part enables the bottom metal to reflect more light. As is shown in the inserted electric-field distribution in Fig. 4(b), only one resonant peak exists when the electric field distribution profile of the etching ring resonance achieves a dominant point. The electric-field enhancement may arise from the plasmon coherent coupling between the etching ring's inner and outer surfaces [27]. The methane sensitivity increases from 7.30 nm/% to 7.81 nm/%, and the improved structure is beneficial to fast response.

(a)

(b)

Fig. 4 Optical reflection spectrum of: (a) primary structure A_6 and (b) improved structure B_6 .

In order to better evaluate the influence of geometric parameters on the sensing performance, we perform additional FDTD simulations for etching rings with different radius. After complete calculations, Table 3 exhibits the sensitivities under different radii and comparison with the structure B_6 . With an increase in R_2 , the methane sensitivity first increases and then gradually decreases. The coupling area becomes larger as the outer radius gets larger, but as the distance increases to a certain value, the coherent coupling between the inner and outer sides becomes attenuated. When $R_2 = 300$ nm and $R_1 = 100$ nm , the sensitivity can reach to the

maximum of 7.98 nm/%. In particular, if we choose $R_2 = 300$ nm and $R_1 = 0$ nm , the nanoring becomes a nanodisk, and a sensitivity of 7.89 nm/% is obtained, which is almost the same as the values above. From the viewpoint of the fabrication technique, the fabrication of the improved structure with a nanodisk is much easier than that case of $R_2 = 300$ nm and $R_1 = 100$ nm . Comprehensively considering response speed, electric field strength, and fabrication technique, the structure with a nanodisk of 300 nm radius is singled out for further investigation.

Table 3 Methane sensitivity under the different radius of etching ring and the comparison with structure B_6.

Group number	Outer radius R_2 (nm)	Inner radius R_1 (nm)	Sensitivity (nm/%)	Increased rate (%)
C_1	280	100	7.92	1.4
C_2	300	100	7.98	2.2
C_3	320	100	7.71	−1.3
C_4	340	100	7.52	−3.7
C_5	**300**	**0**	**7.89**	**1.0**

Considering the excellent sensing characteristics of the Fano resonance [28], we intend to introduce the Fano resonance through breaking the nanostructure's symmetry. We add some etching holes on the corner of the top metal of the previous Structure B as shown in Fig. 5 with a fixed radius $r = 100$ nm. We find that the case of one-hole has a higher sensitivity, which may originate from the highest asymmetry parameter and relative Fano resonance. In asymmetric structures, the line-shape and resonant position of the Fano resonance can be adjusted by the geometry of the structure. This tunability makes the Fano resonance particularly interesting for different sensing applications. As the Fano resonance superimposes the original plasmon resonance, the filed intensity excited by the LSPR increases. The resonant peak will have an obvious shift as gas concentration varies. The sensing performance can be significantly improved. It can be seen from Fig. 6(a) that there exist two modes, which are labeled as Mode 1 and Mode 2. The reflection at the resonant wavelength of Mode 2 is rather small which is more beneficial for the detection. Figure 6(b) proves that a higher gas sensitivity can be achieved. The comparison of gas sensitivity with the symmetric structure C_5 is listed in Table 4.
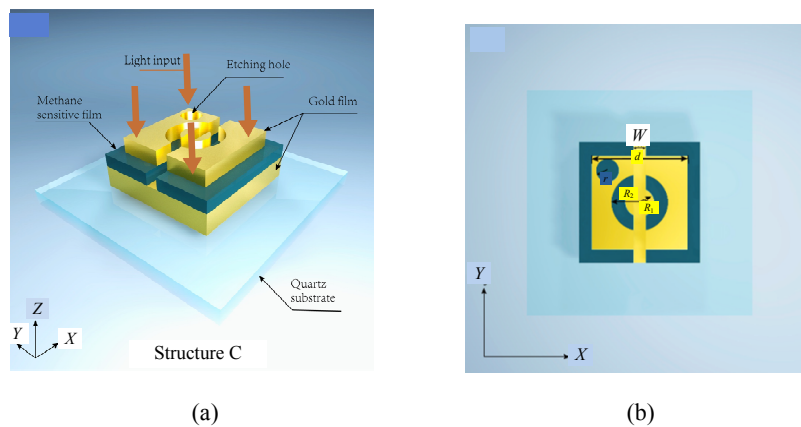

(a)   (b)

Fig. 5 Schematic diagram of the asymmetric structure: (a) 3D view and (b) top view.

(a)   (b)
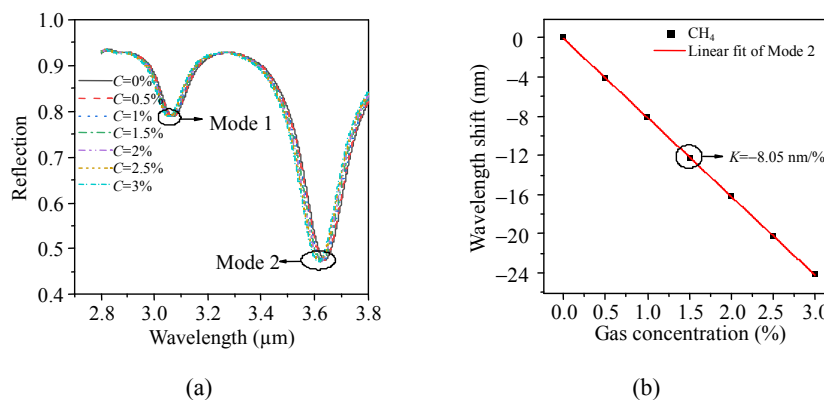
Fig. 6 Reflection spectra of (a) the asymmetric structure and the wavelength-shifts of (b) methane concentrations.

Table 4 Comparison between the asymmetric structure and the symmetric structure C_4.

Structure type	Hole radius r (nm)	Sensitivity (nm/%)	Increased rate (%)
Symmetric	0	7.52	7.0
Asymmetrical	100	8.05	

Obviously, a higher sensitivity of 8.05 nm/% can be obtained from this asymmetric structure with only one hole on the left corner. The methane sensitivity increases by 7.0% compared with the previous one, as is shown in Table 4. It is worth pointing out that the above conclusions are based on the structure C_4, which corresponds to the minimum value in Table 3. After the introduction of the Fano resonance, the asymmetric structure with the minimum sensitivity can generate a higher sensitivity than the maximum sensitivity in the previous structure. Consequently, for the optimized structure C_5 that has acquired the maximum sensitivity of 7.89 nm/%, a final sensitivity of 8.421 nm% can be achieved similarly.

3. Results and expansion

3.1 Sensing results

After comprehensive optimization and the introduction of the Fano resonance for the proposed nanostructure, the methane sensitivity can reach up to 8.421 4 nm/%. Compared with the original structure, the improved structure gains a much better enhancement in sensing performance. According to (7), the refractive index of the sensitive-film has a linear relationship with the target gas within a concentration range of 0% – 3.5%. In this case, the demodulation formula for single-gas measurement is shown in (8), where b is the intercept, and the gas sensitivity is $k = 8.421\,4$ nm/% .

$$\Delta\lambda = k \cdot C_{CH_4} + b .\qquad(8)$$

To assess the accuracy of our demodulation method for different gas concentrations, we select four random testing points [a (0.3%), b (0.7%), c (1.8%), and d (2.4%)] and make comparison with theoretical values obtained by (8). The methane concentration is calculated by analyzing the reflection wavelength shift, as shown in Table 5. It presents that the difference between the values of principal values and calculated concentrations is quite small. Therefore, the demodulation method can meet the demand for higher sensitivity and resolution. Table 6 shows the sensitivity comparison between the proposed structure and other reported sensors. Obviously, the sensitivity has a significant improvement. Different from the gas sensors based on the SPR, we adopt an MDM structure to generate the LSPR effect. A great electromagnetic field occurs at the gas-sensitive film due to the antiparallel surface currents between the top and bottom metals, and the electric-field enhancement also occurs in the groove and etching ring. Then, the sensitivity can be improved through such electric-field enhancements. In the proposed MDM structure, the middle dielectric is a methane-sensitive film, which only reacts to methane but not to other gases. The proposed structure has wide applications range and only needs replacing the dielectric with other gas-sensitive films. In fact, such a structure can be extended to an array to measure multiple gases. The selective detection of gas mixtures can be achieved by applying corresponding gas-sensitive films to the array.

Table 5 Values of the calculated results.

Testing points	Theoretical values	Wavelength shifts	Calculated value	Errors rate
a	0.7	−5.73	0.6995	0.07%
b	1.4	−11.43	1.3763	1.69%
c	2.2	−18.26	2.1874	0.57%
d	3.1	−26.19	3.1290	0.93%

Table 6 Comparison of methane sensitivity to reported methane sensors.

No.	Type	Sensitivity (nm/%)	Reference
1	PCF-SPR	0.540	Yang *et al.* [8]
2	PCF-SPR	1.078	Yang *et al.* [9]
3	PCF-SPR	1.990	Liu *et al.* [10]
4	LSPR	1.040	Liu *et al.* [21]
5	PCF-LPG	2.500	Yang *et al.* [29]
6	Proposed sensor	8.421	

3.2 Analysis and exploration

The proposed nanostructure not only can serve as a gas sensor, but also has significant applications in background refractive index measurement. Based on the asymmetric structure, the influence of various dielectric spacers on the background refractive index (RI) sensitivity are investigated, such as MgF_2, Al_2O_3, SiO_2, and TiO_2 [30]. The refractive indices of MgF_2, Al_2O_3, SiO_2, and TiO_2 are 1.37, 1.75, 1.4, and 2.407, respectively. Figure 7 shows the reflection spectra of the MDM structure with MgF_2, Al_2O_3, SiO_2, and TiO_2, respectively. The inserted illustrations are the electric-field distributions of the MDM structure with different dielectrics at the resonant wavelength. The reflection spectra and electric enhanced distribution of the structure with MgF_2 are approximatively the same as that case of SiO_2. Therefore, the RI sensitivities of the two RI sensors are 554.0 nm/RIU and 548.9 nm/RIU, respectively. Figure 7 also shows that the reflection spectra of the nanostructure with TiO_2 have increased to some extent. The intensity of the electric field is weaker than those of MgF_2 and SiO_2, which is a reason for the lower RI sensitivity. Similarly, the electric field strength of nanostructure with Al_2O_3 is also weaker than those of other cases. Figure 8(a) demonstrates that the coupling peak has a red-shift with an increase in the surrounding refractive index. The phenomenon could be effectively explained by the following reasons. The RI increases from 1.34 to 1.37, a decrease in total dipole component and radiant scattering appears in nanostructure [31, 32].
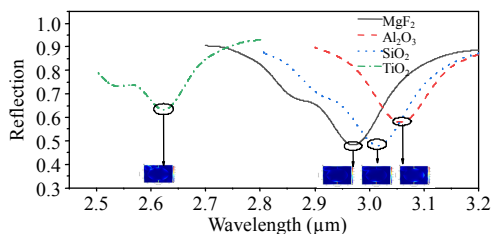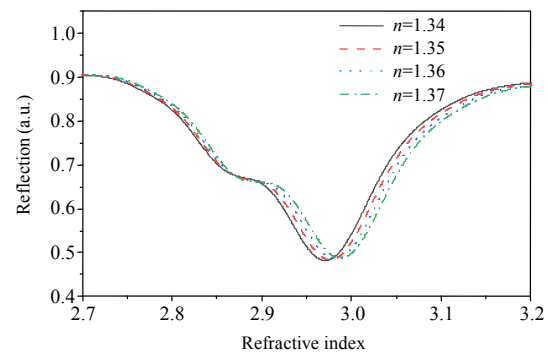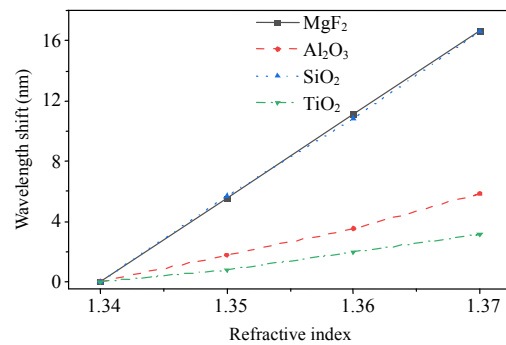

Fig. 7 Reflection spectra of the MDM structure with a dielectric of MgF_2 (black line), SiO_2 (blue line), Al_2O_3 (red line), and TiO_2 (green line), respectively. Insert illustration: electric field distribution of MDM structure with four dielectrics at their individual resonant wavelength.

(a)

(b)

Fig. 8 Reflection spectra of the asymmetric structure with MgF_2 under different background refractive indices (a) and wavelength-shifts of the structure with four different dielectrics (b).

The demodulation formula for the individual sensor with a different spacer is similar to the above methane sensor. Based on the results from Fig. 8(b), the corresponding components of the matrix are demonstrated in Table 7. The RI sensitivity and correlation coefficient of the identical structure with MgF_2 are the highest. We also investigate the RI sensitivity of the proposed several structures with MgF_2, and the comparison are demonstrated in Table 8. It is discovered that Structure A at $w = 20$ nm obtains a better RI sensing performance (648 nm/RIU). This sensing method enables us to have more choices in biosensor and chemical applications.

Table 7 Corresponding elements of the demodulation matrix for four refractive index sensors with different dielectrics.

Dielectric type	RI sensitivity k (nm/RIU)	Correlation coefficient R^2 (%)
MgF_2	554.0	99.99
Al_2O_3	193.4	99.16
SiO_2	548.9	99.93
TiO_2	106.3	98.80

Table 8 RI sensitivity of the proposed different structures with MgF_2.

Structure type	Slit width w (nm)	Outer radius R_2 (nm)	Inner radius R_1 (nm)	RI sensitivity k (nm/RI)	Correlation coefficient R^2 (%)
Structure A	0	0	0	308	100.00
	20	0	0	648	99.99
Structure B	0	240	100	357.6	100.00
	20	240	100	541.5	99.93
		300	0	581.4	99.91
Structure C	20	300	0	554.0	99.99

4. Conclusions

The plasmon resonance characteristics and sensing performance of an asymmetric MDM structure are systematically investigated by the FDTD method. The sensitivity is substantially improved by optimizing our structure, including adding a ring hole in the center and breaking the structure's symmetry. After a series of optimizing processes, the maximum sensitivity of 8.4214 nm/% can be achieved. The proposed method provides a new way for gas detection through the combined use of the MDM structure and Fano resonance. The nanostructure can also be applied to biotechnology and chemical detection as long as the appropriate dielectric is selected as the middle spacer.

Acknowledgment

References

[1] C. Liu, L. Yang, W. Su, F. Wang, T. Sun, Q. Liu, *et al.*, "Numerical analysis of a photonic crystal fiber based on a surface plasmon resonance sensor with an annular analyte channel," *Optics Communications*, 2017, 382: 162–166.

[2] M. Seifouri, M. A. Rouini, and S. Olyaee, "Design of a surface plasmon resonance biosensor based on photonic crystal fiber with elliptical holes," *Optical Review*, 2018, 25(5): 555–562.

[3] G. An, S. Li, W. Qin, W. Zhang, Z. Fan, and Y. Bao, "High-sensitivity refractive index sensor based on D-shaped photonic crystal fiber with rectangular lattice and nanoscale gold film," *Plasmonics*, 2014, 9(6): 1355–1360.

[4] M. Chamanzar, Z. Xia, S. Yegnanarayanan, and A. Adibi, "Hybrid integrated plasmonic-photonic waveguides for on-chip localized surface plasmon resonance (LSPR) sensing and spectroscopy," *Optics Express*, 2013, 21(26): 32086–32098.

[5] J. Chen, Q. Zhang, C. Peng, C. Tang, X. Shen, L. Deng, *et al.*, "Optical cavity-enhanced localized surface plasmon resonance for high-quality sensing," *IEEE Photonics Technology Letters*, 2018, 30(8): 728–731.

[6] S. Tajik and Z. Atlasbaf, "Investigating extraordinary optical transmission and sensing performance through periodic bilayer magneto-plasmonic structure," *Journal of Applied Physics*, 2020, 127(2): 023102.

[7] S. I. Bozhevolnyi, V. S. Volkov, E. Devaux, J. Y. Laluet, and T. W. Ebbesen, "Channel plasmon subwavelength waveguide components including interferometers and ring resonators," *Nature*, 2006, 440(7083): 508–511.

[8] J. C. Yang, X. Che, R. Shen, C. Wang, X. M. Li, and W. M. Chen, "High-sensitivity photonic crystal fiber long-period grating methane sensor with cryptophane-A-6Me absorbed on a PAA-CNTs/PAH nanofilm," *Optics Express*, 2017, 25(17): 20258–20267.

[9] J. C. Yang, L. Zhou, X. Che, J. Huang, X. M. Li, and W. M. Chen, "Photonic crystal fiber methane sensor based on modal interference with an ultraviolet curable fluoro-siloxane nano-film incorporating cryptophane A," *Sensors And Actuators B: Chemical*, 2016, 235: 717–722.

[10] H. Liu, M. Wang, Q. Wang, H. W. Li, Y. Ding, and C. H. Zhu, "Simultaneous measurement of hydrogen and methane based on PCF-SPR structure with compound film-coated side-holes," *Optical Fiber Technology*, 2018, 45: 1–7.

[11] P. Vasa, W. Wang, R. Pomraenke, M. Lammers, M. Maiuri, C. Manzoni, *et al.*, "Real-time observation of ultrafast Rabi oscillations between excitons and plasmons in metal nanostructures with J-aggregates," *Nature Photonics*, 2013, 7(2): 128–132.

[12] S. M. Jiang, D. J. Wu, Y. Cheng, and X. J. Liu,

"Manipulated localized surface plasmon resonances in silver nanoshells coated with a spherical anisotropic layer," *Chinese Physics B*, 2012, 21(12): 127806.

[13] X. Y. Lu, R. G. Wan, F. Liu, and T. Y. Zhang, "High-sensitivity plasmonic sensor based on perfect absorber with metallic nanoring structures," *Journal of Modern Optics*, 2016, 63(2): 177–183.

[14] X. Q. Xu, X. L. Hu, X. S. Chen, Y. S. Kang, Z. P. Zhang, K. B. Parizi, *et al.*, "Engineering a large scale indium nanodot array for refractive index sensing," *ACS Applied Materials & Interfaces*, 2016, 8(46): 31871–31877.

[15] S. A. Wang, X. H. Sun, M. J. Ding, G. D. Peng, Y. L. Qi, Y. L. Wang, *et al.*, "The investigation of an LSPR refractive index sensor based on periodic gold nanorings array," *Journal of Physics D: Applied Physics*, 2018, 51(4): 045101.

[16] S. B. Malani and P. Viswanath, "Impact of ordering of gold nanohole arrays on refractive index sensing," *Journal of the Optical Society of America B-Optical Physics*, 2018, 35(10): 2501–2508.

[17] T. J. Liu and J. Takahara, "Ultrabroadband absorber based on single-sized embedded metal-dielectric-metal structures and application of radiative cooling," *Optics Express*, 2017, 25(12): A612–A627.

[18] L. Lei, S. Li, H. Huang, K. Tao, and P. Xu, "Ultra-broadband absorber from visible to near-infrared using plasmonic metamaterial," *Optics Express*, 2018, 26(5): 5686–5693.

[19] M. Bazgir, M. Jalalpour, F. B. Zarrabi, and A. S. J. J. O. E. M. Arezoomand, "Design of an optical switch and sensor based on a MIM coupled waveguide using a DNA composite," *Journal of Electronic Materials*, 2020, 49(3): 2173–2178.

[20] C. T. Chou Chao, Y. F. Chou Chau, and H. P. Chiang, "Highly sensitive metal-insulator-metal plasmonic refractive index sensor with a centrally coupled nanoring containing defects," *Journal of Physics D: Applied Physics*, 2021, 54(11): 115301.

[21] R. A. Mahmud, M. O. Faruque, and R. H. J. O. C. Sagor, "A highly sensitive plasmonic refractive index sensor based on triangular resonator," *Optics Communications*, 2021, 483: 126634.

[22] R. Singh, I. Al-Naib, W. Cao, and C. Rockstuhl, "The Fano resonance in symmetry broken terahertz metamaterials," *IEEE Transactions on Terahertz Science & Technology*, 2013, 3(6): 820–826.

[23] J. Q. Wang, C. Z. Fan, J. N. He, P. Ding, E. J. Liang, and Q. Z. Xue, "Double Fano resonances due to interplay of electric and magnetic plasmon modes in planar plasmonic structure with high sensing sensitivity," *Optics Express*, 2013, 21(2): 2236–2244.

[24] H. Liu, C. Chen, Y. Zhang, B. Bai, and S. Tang, "A high-sensitivity methane sensor with localized surface plasmon resonance behavior in an improved hexagonal gold nanoring array," *Sensors*, 2019, 19(21): 4803.

[25] S. Wang, X. H. Sun, W. Y. Li, W. Liu, L. Jiang, and J. Han, "Fabrication of photonic quasicrystalline structures in the sub-micrometer scale," *Superlattices and Microstructures*, 2016, 93: 122–127.

[26] B. F. Chen, C. S. Lee, and R. L. Elsberry, "On tropical cyclone size and intensity changes associated with two types of long-lasting rainbands in monsoonal environments," *Geophysical Research Letters*, 2014, 41(7): 2575–2581.

[27] X. He, N. O'Keefe, Y. J. Liu, D. C. Sun, H. Uddin, A. Nirmalathas, *et al.*, "Transmission enhancement in coaxial hole array based plasmonic color filter for image sensor applications," *IEEE Photonics Journal*, 2018, 10(4): 1–9.

[28] B. Luk'yanchuk, N. I. Zheludev, S. A. Maier, N. J. Halas, P. Nordlander, H. Giessen, *et al.*, "The Fano resonance in plasmonic nanostructures and metamaterials," *Nature Materials*, 2010, 9(9): 707–715.

[29] J. Yang, L. Zhou, J. Huang, C. Tao, X. Li, and W. Chen, "Sensitivity enhancing of transition mode long-period fiber grating as methane sensor using high refractive index polycarbonate/cryptophane A overlay deposition," *Sensors & Actuators B: Chemical*, 2015, 207: 477–480.

[30] J. Kischkat, S. Peters, B. Gruska, M. Semtsiv, and W. T. Masselink, "Mid-infrared optical properties of thin films of aluminum oxide, titanium dioxide, silicon dioxide, aluminum nitride, and silicon nitride," *Applied Optics*, 2012, 51(28): 6789–6798.

[31] J. Aizpurua, P. Hanarp, D. S. Sutherland, M. Kll, G. W. Bryant, and G. D. A. Fj, "Optical properties of gold nanorings," *Physical Review Letters*, 2003, 90(5): 057401.

[32] N. Liu, M. Mesch, T. Weiss, M. Hentschel, and H. Giessen, "Infrared perfect absorber and its application as plasmonic sensor," *Nano Letters*, 2010, 10(7): 2342–2348.